Scattering of weak low-frequency light by three-level systems

M. Berent and R. Parzyński

Faculty of Physics, Adam Mickiewicz University, Umultowska 85, 61-614 Poznań, Poland

(Received 22 June 2009; published 24 September 2009)

We calculate analytically both coherent and incoherent parts of the total spectrum of light scattered by a three-level system in either lambda or ladder configurations. The spectrum is restricted to the cases of the incident light pulse weakly depopulating the initial level and of the carrier frequency much lower than the excitation frequency in the system. We give special attention to the spectra under the conditions of different multiphoton resonances in the system and emphasize the effects resulting from the presence of the third level. The analytic theory is shown to explain the numerically calculated spectra as far as the number of frequency components, their positions in the spectrum, relative intensities, and sensitivity to the pulse shape are concerned.

I. INTRODUCTION

Since 2002, a series of theoretical papers has been published concerning multiphoton excitation in specific three-level systems [1–4]. The specificity of the systems was that, first of all, they contained a pair of perfectly or nearly degenerate excited states separated from the ground state by many photons. Moreover, the excited states were either dipole coupled to each other or had nonzero mean dipole moments. In the former case, the chain of the electric-dipole couplings in the three-level system formed the Γ-type configuration, while in the latter one the V-type configuration. For both configurations, the dynamics of the system was found to reduce to that of the two-level Rabi system but with a generalized Rabi frequency being nonlinearly dependent on the electric-field amplitude of the exciting photon beam. Specifically, this dependence was given by the Bessel function of the same order as that of the multiphoton resonance and that of the argument including the coupling between (or in) the excited states weighted by the field frequency. It was shown that the excited-state dipole couplings result in substantial enhancement of both multiphoton excitation from the ground state and harmonic generation.

In the present paper we deal with a different three-level system obtained, formally, from the above Γ-type configuration by separating the excited states by a number of photons. As a result, all states of the system of interest, with the dipole couplings between them, form either the lambda (Λ) or ladder configurations. Mathematically, this system is more challenging because its population dynamics cannot be reduced to that of the two-level system [5]. Thus, the present paper goes beyond the fundamental problem of the two-level system in an oscillating field extensively studied in the past in the context of, e.g., the generation of harmonics of the incident light by atoms, molecular ions, double-well potentials, and semiconductors [6–18]. Though being a serious approximation, the two-level model has succeeded in reproducing qualitatively many features of the experimental harmonic spectra such as, e.g., the broad plateau, the cutoff frequency, and the dependence of the spectra on the carrier-envelope phase shift of the extremely short light pulses available at present. Obviously, by the two-level approximation

many effects in the spectra are, however, hidden and the aim of our three-level model is to indicate and explain some of these effects. In our formulation, this three-level model has the advantage of being analytically solvable in a relatively simple way due to two main assumptions. The first assumption is that the frequency of the incident light is small compared to the transition frequency between the different-parity ground and excited levels in the model. A single photon from the light beam is thus far from resonance with this transition; however it has such an energy that many of these photons (odd integer) nearly cover this transition. Subsequent odd-photon resonance between the opposite-parity excited levels is also allowed as well as an even-photon resonance between the same-parity levels of the model. From a variety of levels in a real system these multiphoton resonances are believed to pick out the three essential levels reducing to them the excitation dynamics to the first approximation. The simplest practical realization of this model can be the first three levels in the hydrogen atom, i.e., the $1S$, $2P$, and $3S+3D$ ones. In the above three-level ladder configuration, the light beam of frequency being in 15-photon resonance with the $1S \rightarrow 2P$ transition is, at the same time, close to three-photon resonance with the $2P \rightarrow 3S+3D$ transition. The same can be said about the lowest three electronic levels in the H_2^+ molecular ion, namely, the $1\sigma_g$, $1\sigma_u$, and $2\sigma_g$ ones at internuclear separations close to the equilibrium distance equal to 2 a.u. (Fig. 1 in [9]). In this case, the light beam in, e.g., 9 (15)-photon resonance with the lower $1\sigma_g \rightarrow 1\sigma_u$ transition is, accidentally, in nearly 7 (11)-photon resonance with the upper $1\sigma_u \rightarrow 2\sigma_g$ transition. It seems that the lowest levels in the hydrogen atom can also serve for a realization of the three-level lambda configuration. For instance, the light beam in 4 (6)-photon resonance with the $1S \rightarrow 2S$ transition is nearly in 5 (7)-photon resonance with the $1S \rightarrow 3P$ transition. Thus, at these frequencies the coupling chain $1S \rightarrow 3P \rightarrow 2S$ forms the required lambda scheme, which should not be perturbed substantially by the $2P$ state because this state, as compared to the $3P$ one, is farther from odd-photon resonance with the ground state. However, to minimize a possible effect of higher-lying states in the real system we make the second assumption, i.e., that of weak excitation
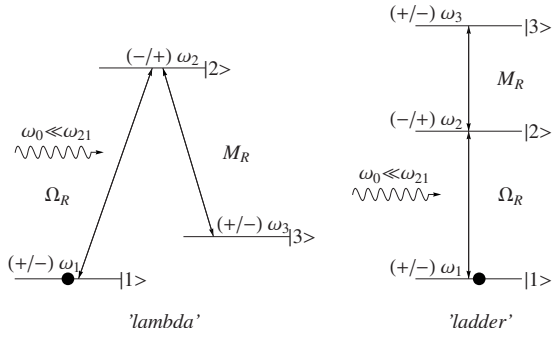
FIG. 1. Electric-dipole couplings in a three-level system driven by a laser beam of frequency ω_0 much smaller than the transition frequency $\omega_{21} = \omega_2 - \omega_1$. The dotted points to the localization of the initial population, the signs $\pm$ to the parity of states, ω_j (with $j = 1-3$) to the state eigenfrequencies, and Ω_R and M_R to the time-independent Rabi frequencies.

guaranteed by relatively weak field leaving the system mostly in its initial state throughout the whole interaction time. Under the above assumptions we calculate analytically the spectrum of light scattered by the three-level system with emphasis put on the effects originated in the third level. The analytical spectrum, when compared with that obtained by a fully numerical procedure, proves a good quality of our analytic approach. In contrast to the two-level calculations [6,7,9–18], the spectrum is understood here as the total spectrum, i.e., that composed of both the coherent and incoherent parts, and one particular aim of the paper is to point to a substantial effect of the latter part in the total spectrum. In a simple way, we also show the effect of the shape of the pulsed field on some frequency components in the spectrum. It is thus evident that the present paper differs in many points from that of Caldara and Fiordilino [19] for the Λ system because the latter paper brings purely numerical results concerning the coherent part of the spectrum only.

Our paper is organized as follows. In Sec. II, we present the model, define the total spectrum, and give the starting equations for the population dynamics. Section III is devoted to the coherent part of the spectrum calculated analytically from two coupled equations of motion for the appropriately defined ratios of the level-population amplitudes. The found analytic solution serves then as a basis to show and discuss the effects in the coherent spectrum caused by the third level. Using the approach of Sec. III, in Sec. IV we calculate analytically the incoherent part of the spectrum and, then, the total spectrum. Finally, we give brief summary in Sec. V.

II. MODEL AND BASIC EQUATIONS

Figure 1 shows the three-level system in either the lambda or ladder configuration. The two configurations are realized by choosing positive or negative, respectively, frequency difference, $\omega_{23} = \omega_2 - \omega_3$. The bare states of the model have well defined parities, "$\pm$," with the parities of states $|1\rangle$ and $|3\rangle$ being the same and opposite to the parity of state $|2\rangle$. The system is exposed to a single laser beam, linearly polarized along the z axis, of frequency ω_0 much lower than the

transition frequency $\omega_{21} = \omega_2 - \omega_1$ from initial state $|1\rangle$ to excited state $|2\rangle$, i.e., $\omega_0 \ll \omega_{21}$. We take the electric field of light in the classical form, $E(t) = E_0 f(t)\cos(\omega_0 t)$, where E_0 stands for the amplitude and $0 \leq f(t) \leq 1$ for the normalized pulse-shape function. This field couples the levels through the electric-dipole interaction $V(t) = -ezE(t)$. The coupling is assumed to be weak in the sense of weak depopulation of the initial state. With this interaction, we define the instantaneous Rabi frequencies for the 1-2 and 2-3 couplings, namely, $\Omega(t) = -V_{12}(t)/\hbar$ and $M(t) = -V_{23}(t)/\hbar$, where $V_{jk}(t)$ are the appropriate matrix elements of the interaction. Explicitly, $\Omega(t) = \Omega_R f(t)\cos(\omega_0 t)$ and $M(t) = M_R f(t)\cos(\omega_0 t)$, where $\Omega_R = \mu_{12}E_0/\hbar$ and $M_R = \mu_{23}E_0/\hbar$ are the conventional time-independent Rabi frequencies while $\mu_{jk} = \langle j|ez|k\rangle$ is the matrix element of the dipole transition $j \to k$.

In this paper, we shall calculate analytically the total spectrum of light scattered by the system of Fig. 1. We use the definition of the total spectrum, $S(\omega)$, based on the correspondence principle connecting the classical and quantum physics. All details of this definition are given in the original papers [20,21], where the appropriate quantum spectrum is called the correspondence principle spectrum. Shortly, the quantum definition of the spectrum is obtained from the classical definition (the squared modulus of the Fourier transform of the scattered electric field) by, first, replacing the classical dynamical variables by the corresponding operators and, then, taking the expectation value in the initial state of the system (Eqs. (2.1)–(2.3) in [21]). Such a procedure leads directly to the spectrum $S(\omega)$ expressed by the two-dimensional Fourier transform of the standard two-time dipole correlation function (Eqs. (2.4), (3.3), and (B4) in [21]). Finally, after inserting the unit projector $\Sigma_j|j\rangle\langle j|$ into the correlation function and using the time evolution operator $U(t)$ when going from the Heisenberg to the Schrödinger pictures one obtains the original Eqs. (3.10) and (3.11) in [21] defining the correspondence principle spectrum $S(\omega)$ from a multilevel system. For the three-level model of Fig. 1, this definition of $S(\omega)$ reduces to

$$S(\omega)/\omega^4 = \sum_{j=1}^{3} \left| \int_0^{t_p} dt\, e^{i\omega t} \langle \Psi_j(t)|ez|\Psi_1(t)\rangle \right|^2, \quad (1)$$

where t_p is the duration of the incoming laser pulse and $\Psi_j(t)$ stands for the Schrödinger wave function of the laser-driven three-level system beginning its evolution in the bare eigenstate $|j\rangle$ at $t=0$, i.e., $|\Psi_j(0)\rangle = |j\rangle$. The diagonal term, $j=1$ in Eq. (1), defines what is referred to as the coherent part of the spectrum, $S_c(\omega)$, and the rest, $S(\omega) - S_c(\omega) = S_{inc}(\omega)$, is the incoherent part. The coherent part is the spectrum of the average dipole moment, while the incoherent part is the spectrum of the quantum dipole fluctuations. However, because we work with the Schrödinger equation instead the master equation, the spectrum resulting from Eq. (1) is correct only under the assumption that the duration of the incident light pulse is shorter than the excited-state lifetimes. Typically we will concentrate on pulses of the duration equal to 30 optical cycles when giving the representative spectra.

From Eq. (1), one can calculate the spectrum with an accuracy depending on our knowledge concerning the Schrödinger function $\Psi_j(t)$. According to Fig. 1, we take $\Psi_j(t)$ as an expansion in terms of the bare states $|k\rangle$, namely, $\Psi_j(t) = \Sigma_{k=1}^3 b_{kj}(t)|k\rangle$, where $b_{kj}(t)$ is the time-dependent population amplitude of state $|k\rangle$ provided that initially ($t=0$) the system was in state $|j\rangle$. These amplitudes determine completely the time evolution of the core of the Fourier integral,

$$\langle \Psi_j(t)|ez|\Psi_1(t)\rangle = \sum_{k=1}^{3} \sum_{l=1}^{3} b_{kj}^* b_{l1}\mu_{kl} = \mu_{12}(b_{1j}^* b_{21} + b_{2j}^* b_{11})$$
$$+ \mu_{23}(b_{2j}^* b_{31} + b_{3j}^* b_{21}), \qquad (2)$$

where we have assumed that μ_{kl} are real and, also, used the conditions of nonvanishing of μ_{kl}. From the Schrödinger equation, the state population amplitudes are then found to satisfy the set of coupled differential equations,

$$i\frac{db_{1j}}{dt} = \omega_1 b_{1j} - \Omega(t)b_{2j}, \qquad (3a)$$

$$i\frac{db_{2j}}{dt} = \omega_2 b_{2j} - \Omega(t)b_{1j} - M(t)b_{3j}, \qquad (3b)$$

$$i\frac{db_{3j}}{dt} = \omega_3 b_{3j} - M(t)b_{2j}. \qquad (3c)$$

III. COHERENT SPECTRUM

To calculate the coherent part of the spectrum, $S_c(\omega)$, one needs to put $j=1$ in Eqs. (1), (2), and (3a)–(3c). As a result,

$$S_c(\omega)/\omega^4 = \left| \int_0^{t_p} dt e^{i\omega t} d(t) \right|^2 = |d(\omega)|^2, \qquad (4)$$

with $d(\omega)$ being the finite-time Fourier transform of the dipole expectation value $d(t) = \langle \Psi_1(t)|ez|\Psi_1(t)\rangle$. This value is to be calculated under the initial condition indicated by the black dot in Fig. 1. In terms of the state population amplitudes, the dipole expectation value reads

$$d(t) = 2\mu_{12} \text{Re}(b_{11}^* b_{21}) + 2\mu_{23} \text{Re}(b_{21}^* b_{31}), \qquad (5)$$

as resulting from Eq. (2).

However, instead of the three amplitudes b_{k1}, we prefer to work with two new variables defined as the appropriate ratios of the amplitudes, namely, $r = b_{21}/b_{11}$ and $\rho = b_{31}/b_{11}$. In terms of these ratios, we rewrite Eq. (5) for the dipole expectation value as

$$d(t) = 2\mu_{12}|b_{11}|^2 \text{Re}(r) + 2\mu_{23}|b_{21}|^2 \text{Re}(\rho/r)$$
$$= 2\mu_{12}\frac{\text{Re}(r)}{1+|r|^2+|\rho|^2} + 2\mu_{23}\frac{\text{Re}(r^*\rho)}{1+|r|^2+|\rho|^2}, \qquad (6)$$

where the denominators in the last line result from the probability conservation law, $|b_{11}|^2 + |b_{21}|^2 + |b_{31}|^2 = 1$, and the definitions of r and ρ. By differentiating once both r and ρ,

the ratios are found from Eqs. (3) to satisfy the set of coupled differential equations,

$$i\frac{dr}{dt} = (r^2 - 1)\Omega(t) + \omega_{21}r - M(t)\rho, \qquad (7a)$$

$$i\frac{d\rho}{dt} = [\omega_{31} + \Omega(t)r]\rho - M(t)r. \qquad (7b)$$

For a known $r(t)$, Eq. (7b) is an inhomogeneous linear first-order differential equation of the form $\frac{du}{dt} + P(t)u = Q(t)$ with the solution [22]

$$u(t) = \frac{1}{z(t)}\left(\int_{t_0}^t Q(t')z(t')dt' + u(t_0) \right), \qquad (8)$$

where $z(t) = \exp[\int_{t_0}^t P(t')dt']$ and $u(t_0)$ is the value of u at the initial time $t=t_0$. We will apply Eq. (8) many times throughout this paper.

A. Weak-field low-frequency excitation

In the following, we shall consider a special case of weak depopulation of the initial state, $|r| \ll 1$. Alternatively, it will be referred to as the weak-excitation case. In this case, one can neglect the term $M(t)b_{31}$ in Eq. (3b), resulting in the neglect of the last term on the right-hand side of Eq. (7a), $M(t)\rho$. Then, Eq. (7a) is decoupled from Eq. (7b) and simplified to the form

$$i\frac{dr}{dt} = (r^2 - 1)\Omega(t) + \omega_{21}r. \qquad (9)$$

It is nontrivial (quadratically nonlinear) Riccati-type equation for a two-level system [17,18]. In the weak-excitation limit, Eq. (9) can be solved by successive approximations. In the zero-order approximation, we neglect the quadratic term, r^2, obtaining the equation

$$i\frac{dr_0}{dt} = \omega_{21}r_0 - \Omega(t). \qquad (10)$$

To have a solution slightly better than r_0 we then put $r = r_0 + r_1$ into Eq. (9), assuming $|r_1| \ll |r_0|$. Under this assumption, we ignore the minor term quadratic in r_1 in Eq. (9) and also use the zero-order equation [Eq. (10)]. Along this line we obtain the equation for small correction r_1,

$$i\frac{dr_1}{dt} = [\omega_{21} + 2r_0\Omega(t)]r_1 + r_0^2\Omega(t). \qquad (11)$$

Equations (10) and (11) form a linearized approximation to Eq. (9) at $|r| \ll 1$. Finally, we find ρ from the simplified version of Eq. (7b),

$$i\frac{d\rho}{dt} = [\omega_{31} + \Omega(t)r_0]\rho - M(t)r_0. \qquad (12)$$

Equations (10)–(12) have their solutions in the form of Eq. (8) with appropriately identified $P(t)$ and $Q(t)$ functions. Specifically

$$r_0 = ie^{-i\omega_{21}t} \int_{t_0}^{t} \Omega(t')e^{i\omega_{21}t'}dt', \qquad (13)$$

$$r_1 = -ie^{-i[\omega_{21}t+2A_0(t)]} \int_{t_0}^{t} r_0^2(t')\Omega(t')e^{i[\omega_{21}t'+2A_0(t')]}dt', \qquad (14)$$

$$\rho = ie^{-i[\omega_{31}t+A_0(t)]} \int_{t_0}^{t} r_0(t')M(t')e^{i[\omega_{31}t'+A_0(t')]}dt', \quad (15)$$

where

$$A_0(t) = \int_{t_0}^{t} r_0(t')\Omega(t')dt'. \qquad (16)$$

As an example, we calculate the integrals in Eqs. (13)–(16) assuming square-envelope laser pulse [$f(t)=1, t_0 =0$]. This choice leads to

$$r_0 = \frac{\Omega_R}{2}e^{-i\omega_{21}t}\left(\frac{e^{i\Delta^+ t}-1}{\Delta^+} + \frac{e^{i\Delta t}-1}{\Delta}\right), \qquad (17)$$

$$A_0 = \frac{\Omega_R^2}{4\Delta\Delta^+}\left\{2\omega_{21}\left[t + \frac{\sin(2\omega_0 t)}{2\omega_0} - \frac{\sin(\Delta t)}{\Delta} - \frac{\sin(\Delta^+ t)}{\Delta^+}\right]\right.$$
$$+ i\left\{\frac{(\Delta^+)^2 + \Delta^2 + \Delta\Delta^+}{\Delta\Delta^+} - 2\omega_{21}\left[\frac{\cos(\Delta t)}{\Delta} + \frac{\cos(\Delta^+ t)}{\Delta^+}\right]\right\}$$
$$\left. + \cos(2\omega_0 t)\right\}\right\}, \qquad (18)$$

where $\Delta = \omega_{21} - \omega_0$ and $\Delta^+ = \omega_{21} + \omega_0$. Obviously, the use of the above r_0 and A_0 will result in very complicated final expressions for r_1 [Eq. (14)] and ρ [Eq. (15)]. However, in the case of our interest, i.e., that of low-frequency excitation ($\omega_0 \ll \omega_{21}$), when a number of laser photons ω_0 are needed to cover the distance ω_{21}, considerable simplifications are possible. Since then $\Delta^+ \approx \Delta \approx \omega_{21}$, one arrives at the approximate expressions

$$r_0 = \frac{\Omega_R}{\omega_{21}}[\cos(\omega_0 t) - e^{-i\omega_{21}t}] \qquad (19)$$

and

$$A_0 = \frac{\Omega_R^2}{2\omega_{21}}\left(t + \frac{\sin(2\omega_0 t)}{2\omega_0}\right). \qquad (20)$$

It becomes clear from Eq. (19) that to satisfy the weak-excitation condition, $|r| \ll 1$, one needs $\Omega_R/\omega_{21} \ll 1$ limiting the electric-field strength of the laser pulse, E_0. Moreover, the calculation of r_1 and ρ with the use of $A_0(t)$ of Eq. (20) is then much facilitated since we can apply the Fourier-Bessel expansion [23]

$$e^{iqA_0} = e^{iq\Delta_s t/2}e^{x_q \sin(2\omega_0 t)} = e^{iq\Delta_s t/2}\sum_{m=-\infty}^{\infty} J_m(x_q)e^{i2m\omega_0 t}, \qquad (21)$$

where $q=1$ or 2, $\Delta_s = \Omega_R^2/\omega_{21}$ has the meaning of the Stark shift, $x_q = q\Delta_s/(4\omega_0) = q\Omega_R^2/(4\omega_0\omega_{21}) \ll 1$, and $J_m(x_q)$ is the Bessel function of integer order. With this expansion, the integrals in Eqs. (14) and (15) become elementary though their calculation is much time consuming.

To show the effect of the pulse shape we also consider the case of a smooth envelope given by $f(t) = \sin(\Delta_l t)$, where $0 \le t \le t_p$ and $\Delta_l = \pi/t_p$. In this case, the length of the pulse, t_p, determines the full width at half maximum of the pulse by $\Delta t_{1/2} = \frac{2}{3}t_p$. This width translates into the spectral full width at half maximum equal to $\Delta\nu_{1/2} = 1/\Delta t_{1/2} = 3\Delta_l/(2\pi)$. Then r_0 of Eq. (13) takes the form

$$r_0 = \frac{\Omega_R}{2}\left[\frac{\omega_{21}\sin(\omega_0 + \Delta_l)t + i(\omega_0 + \Delta_l)\cos(\omega_0 + \Delta_l)t}{\omega_{21}^2 - (\omega_0 + \Delta_l)^2}\right.$$
$$- \frac{\omega_{21}\sin(\omega_0 - \Delta_l)t + i(\omega_0 - \Delta_l)\cos(\omega_0 - \Delta_l)t}{\omega_{21}^2 - (\omega_0 - \Delta_l)^2}$$
$$\left. + i\left(\frac{\omega_0 - \Delta_l}{\omega_{21}^2 - (\omega_0 - \Delta_l)^2} - \frac{\omega_0 + \Delta_l}{\omega_{21}^2 - (\omega_0 + \Delta_l)^2}\right)e^{-i\omega_{21}t}\right]. \qquad (22)$$

For low-frequency ($\omega_0 \ll \omega_{21}$) many-cycle pulse ($t_p \gg T = 2\pi/\omega_0 \rightarrow \Delta_l \ll \omega_0/2$), the above r_0 converts into

$$r_0 = \frac{\Omega_R}{\omega_{21}}\left(f(t)\cos(\omega_0 t) - i\frac{\Delta_l}{\omega_{21}}e^{-i\omega_{21}t}\right). \qquad (23)$$

In the same limits,

$$A_0 = \frac{\Omega_R^2}{2\omega_{21}}f^2(t)\left(t + \frac{\sin(2\omega_0 t}{2\omega_0}\right). \qquad (24)$$

As compared with Eqs. (19) and (20) for the square-pulse case, the main difference consists of the small factor $\Delta_l/\omega_{21} = (\omega_0/\omega_{21})(\Delta_l/\omega_0) \ll 1$ at $e^{-i\omega_{21}t}$ in Eq. (23) for r_0. This difference in r_0 will produce differences in r_1 and ρ of Eqs. (14) and (15), respectively. As a result, any effect coming from the term proportional to $e^{-i\omega_{21}t}$ in r_0 is expected to be much smaller for a smooth pulse than for a square one.

B. Dipole expectation value

Under the assumed weak-excitation condition, $|r|, |\rho| \ll 1$, the dipole expectation value of Eq. (6) reduces to the three-term sum, $d(t) = d_0(t) + d_1(t) + d_\rho(t)$, where $d_0(t) = 2\mu_{12}\text{Re}(r_0)$, $d_1(t) = 2\mu_{12}\text{Re}(r_1)$, and $d_\rho(t) = 2\mu_{23}\text{Re}(r_0^*\rho)$. Using the square-pulse equations [Eqs. (19)–(21)], these terms are found from Eqs. (13)–(15) in the following analytic forms:

$$d_0(t) = 2\mu_{12}\frac{\Omega_R}{\omega_{21}}[\cos(\omega_0 t) - \cos(\omega_{21}t)], \qquad (25)$$

$$d_1(t) = \frac{\mu_{12}}{4} \frac{\Omega_R^3}{\omega_{21}^2} \sum_{m=-\infty}^{+\infty} \sum_{n=-\infty}^{+\infty} J_n(x_2)(P_m \cos[\omega_{21} - 2(m-n)\omega_0]t$$

$$+ Q_m \cos(\omega_{21} + 2n\omega_0 + \Delta_s)t - R_m \cos[2(m-n)$$

$$+ 1]\omega_0 t + S_m \cos\{2\omega_{21} - [2(m-n)+1]\omega_0\}t), \quad (26)$$

$$d_\rho(t) = \frac{\mu_{23}}{4} \frac{M_R \Omega_R^2}{\omega_{21}^2} \sum_{m=-\infty}^{+\infty} \sum_{n=-\infty}^{+\infty} J_n(x_1) \Bigg\{ T_m \cos[2(m-n)$$

$$+ 1]\omega_0 t - U_m \cos[\omega_{21} + 2(m-n)\omega_0]t + V_m \cos[\omega_{21}$$

$$- 2(m-n)\omega_0]t - W_m \Bigg[\cos\Big([\omega_{31} + (2n-1)]\omega_0 + \frac{\Delta_s}{2} \Big)t$$

$$+ \cos\Big(\omega_{31} + (2n+1)\omega_0 + \frac{\Delta_s}{2} \Big)t$$

$$- 2 \cos\Big(\omega_{23} - 2n\omega_0 - \frac{\Delta_s}{2} \Big)t \Bigg] \Bigg\}. \quad (27)$$

The frequency and field-dependent coefficients in $d_1(t)$ are

$$P_m = 4a_{m-1}[J_{m-1}(x_2) + J_{m+1}(x_2) + 2J_m(x_2)], \quad (28)$$

$$Q_m = (3c_m + 3c_{m-1} + c_{m+1} + c_{m-2} - 4b_m - 4b_{m-1}$$
$$- 4a_m - 8a_{m-1} - 4a_{m-2})J_m(x_2), \quad (29)$$

$$R_m = c_m[3J_m(x_2) + 3J_{m+1}(x_2) + J_{m-1}(x_2) + J_{m+2}(x_2)], \quad (30)$$

$$S_m = 4b_m[J_m(x_2) + J_{m+1}(x_2)], \quad (31)$$

$$a_m = \frac{1}{2(m+1)\omega_0 + \Delta_s}, \quad (32)$$

$$b_m = \frac{1}{\omega_{21} - (2m+1)\omega_0 - \Delta_s}, \quad (33)$$

$$c_m = \frac{1}{\omega_{21} + (2m+1)\omega_0 + \Delta_s}, \quad (34)$$

while those in $d_\rho(t)$ have the forms

$$T_m = f_m[J_m(x_1) + 2J_{m+1}(x_1) + J_{m+2}(x_1)] + f_{m-1}[2J_m(x_1)$$
$$+ J_{m-1}(x_1) + J_{m+1}(x_1)] - 4g_m[J_m(x_1) + J_{m+1}(x_1)], \quad (35)$$

$$U_m = 2f_{m-1}[2J_m(x_1) + J_{m-1}(x_1) + J_{m+1}(x_1)], \quad (36)$$

$$V_m = 2g_m[J_m(x_1) + J_{m+1}(x_1)] + 2g_{m-1}[J_m(x_1) + J_{m-1}(x_1)], \quad (37)$$

$$W_m = (f_m + 2f_{m-1} + f_{m-2} + 2g_m + 2g_{m-1})J_m(x_1), \quad (38)$$

$$f_m = \frac{1}{\omega_{31} + (2m+2)\omega_0 + \frac{\Delta_s}{2}}, \quad (39)$$

$$g_m = \frac{1}{\omega_{23} - (2m+1)\omega_0 - \frac{\Delta_s}{2}}. \quad (40)$$

Except a_m, the coefficients b_m, c_m, f_m, and g_m are seen to have resonance structures. Resonances occur when the total energy of an appropriate number of photons approaches the level separation energy ω_{21}, $|\omega_{31}|$, or $|\omega_{23}|$. In agreement with the multiphoton electric-dipole selection rules, these coefficients allow either odd-photon $1 \rightarrow 2$ and $2 \rightarrow 3$ resonances or even-photon $1 \rightarrow 3$ resonance.

The conclusion from Eqs. (25)–(27) is that, under weak low-frequency excitation by square-envelope pulse of frequency ω_0, the expected frequency components in the coherent part of the spectrum are $(2k+1)\omega_0$, $\omega_{21} \pm 2k\omega_0$, $2\omega_{21} \pm (2k+1)\omega_0$., $\omega_{31} \pm (2k+1)\omega_0$, and $\omega_{23} \pm 2k\omega_0$, in general, where $k = 0, 1, 2, \ldots$. Depending on the specific conditions, only some of the above possible components are predicted to reveal well in the spectrum. In agreement with what was said in the last sentence of Sec. III A, the components $\omega_{21} \pm 2k\omega_0$ and $\omega_{23} \pm 2k\omega_0 = \omega_{21} - \omega_{31} \pm 2k\omega_0$ should be weakened by the factor $(\Delta_l / \omega_{21})^2$ when one uses a smooth pulse [$f(t) = \sin(\Delta_l t)$] instead of a square pulse [$f(t) = 1$].

C. Representative coherent spectra

Because of the weak-field $(\Omega_R / \omega_{21} \ll 1)$ and low-frequency $(\omega_0 \ll \omega_{21})$ assumptions the arguments of the Bessel functions, $x_q = q\Omega_R^2 / (4\omega_0 \omega_{21})$ with $q = 1$ or 2, remain much smaller than 1 justifying the approximation $J_m(x_q) \approx (x_q / 2)^m / m!$ for $m \geq 0$. For negative Bessel indices one should use the relation $J_{-m}(x_q) = (-1)^m J_m(x_q)$ first. This approximation means that we are allowed to retain only those summation indices, m and n, which generate the lowest-order Bessel functions in Eqs. (26) and (27) for $d_1(t)$ and $d_\rho(t)$, respectively.

Far from the odd-photon $1 \rightarrow 2$ resonance, we retain the summation indices which lead to $J_0^2(x_2)$ in $d_1(t)$. Then, due to the low-frequency condition, we approximate $b_m = c_m \approx 1/\omega_{21}$. Also, we neglect Δ_s in the denominator of a_m if $m \neq -1$. As a result, one finds

$$d_1(t) = \frac{\mu_{12}}{2} \Big(\frac{\Omega_R}{\omega_{21}} \Big)^3 \Bigg\{ \frac{\omega_{21}}{\omega_0} \Bigg[\cos(\omega_{21} - 2\omega_0)t - \cos(\omega_{21} + 2\omega_0)t$$

$$- \frac{4\omega_0}{\Delta_s}[\cos(\omega_{21} + \Delta_s)t - \cos(\omega_{21}t)] \Bigg] - 3 \cos(\omega_0 t)$$

$$- \cos(3\omega_0 t) + 2[\cos(2\omega_{21} - \omega_0)t + \cos(2\omega_{21} + \omega_0)t] \Bigg\}. \quad (41)$$

As a matter of fact, $d_0(t)$ of Eq. (25) and $d_1(t)$ of Eq. (41) determine roughly the coherent part of the scaled spectrum, $S_c(\omega)/\omega^4$, from a two-level system (levels 1 and 2 in Fig. 1 only) under weak low-frequency excitation by square-envelope pulse. As seen from $d_0(t)$, this scaled spectrum should be dominated by two well separated frequencies, the laser frequency ω_0 and the transition frequency ω_{21}. The peaks at these positions in the scaled spectrum are of equal

height. From $d_1(t)$ of Eq. (41) one should also expect additional peaks, mainly the satellites of the $1 \rightarrow 2$ transition frequency, $\omega_{21} \pm 2\omega_0$. The satellites have the same height in the scaled spectrum but are lower than the dominant peaks because the ratio $d_1(t)/d_0(t) \approx \Omega_R^2/(4\omega_0\omega_{21}) = x_1 \ll 1$. In the low-frequency part of the spectrum, also weaker third harmonic peak of the laser frequency ($3\omega_0$) should be revealed. The above two-level result agrees with that of Zuo *et al.* [9] obtained by applying the Wentzel-Kramers-Brillouin method when solving approximately the equations for the amplitudes b_{11} and b_{21} [Eqs. (3) with $b_{31}=0$]. On the other hand, the predicted high-frequency components $2\omega_{21} \pm \omega_0$ agree with the numerical result of Caldara and Fiordilino [19].

The effect of the third level of the model from Fig. 1 is nested in $d_\rho(t)$ of Eq. (27) or, more specifically, in the coefficients f_m and g_m defined by Eqs. (39) and (40), respectively. As a special case, let us consider nearly two-photon ω_{31} spacing ($\omega_{31} \approx 2\omega_0$) resulting in the Λ configuration of the levels. At $\omega_{31} \approx 2\omega_0$, the coefficient f_{-2} reaches high value and the dominant terms in $d_\rho(t)$ are those accompanied by the product $f_{-2}J_0^2(x_1)$. Separating these terms and introducing $\delta_0 = \omega_{31} - 2\omega_0$ as the static two-photon detuning for the $1 \rightarrow 3$ transition, one obtains

$$d_\rho(t) = \frac{\mu_{23}}{4}\frac{M_R\Omega_R^2}{\omega_{21}^2}\frac{1}{\delta_0 + \frac{\Delta_s}{2}}\left[\cos(\omega_0 t) - \cos\left(\omega_0 + \delta_0 + \frac{\Delta_s}{2}\right)t\right.$$
$$+ \cos(3\omega_0 t) - \cos\left(3\omega_0 + \delta_0 + \frac{\Delta_s}{2}\right)t + 2\cos\left(\omega_{21}\right.$$
$$\left.\left. - 2\omega_0 - \delta_0 - \frac{\Delta_s}{2}\right)t - 2\cos(\omega_{21} - 2\omega_0)t\right]. \quad (42)$$

When $\delta_0 \rightarrow 0$, the factor before the bracket increases and becomes comparable with that in $d_0(t)$ of Eq. (25), i.e., even higher than that in $d_1(t)$ of Eq. (41). Thus, for $\delta_0 \rightarrow 0$, the third level is seen to change appreciably the scaled spectrum of the two-level system. Even more dramatic changes are expected when $\delta_0 \rightarrow -\Delta_s/2$. The main changes should consist of introducing asymmetry in the heights of the satellites $\omega_{21} \pm 2\omega_0$ of the transition frequency ω_{21} in enhancing the third harmonic and in introducing doublet structures around the frequencies ω_0, $3\omega_0$, and $\omega_{21}-2\omega_0$. All these effects, originating in the third level, are clearly seen in Fig. 2. Figure 2(a) corresponds to the two-level system and serves as a reference point for comparisons, while Figs. 2(b) and 2(c) to the three-level lambda systems characterized by different values of the two-photon $1 \rightarrow 3$ detuning, $\delta_0 = \omega_{31} - 2\omega_o$, with positive frequency difference ω_{31}. The solid curves were obtained by using analytic equations [Eqs. (25)–(27)], while the dotted curves result from numerical solution of Eqs. (3). In Fig. 2(a), the analytic and numerical curves coincide almost perfectly. In Fig. 2(b), the agreement between the approximate analytic curve and the numerical one is seen to be good as far as the number of peaks, their positions, and relative heights are concerned. In this case, the weak-excitation condition was satisfied well for all times [$|r(t)|^2 \leq 0.006$ and $|\rho(t)|^2 \leq 0.0025$]. However, for the parameters of Fig. 2(c) this condition was poorly satisfied [$|r(t)|^2 \leq 0.009$ and

(a)

(b)

(c)
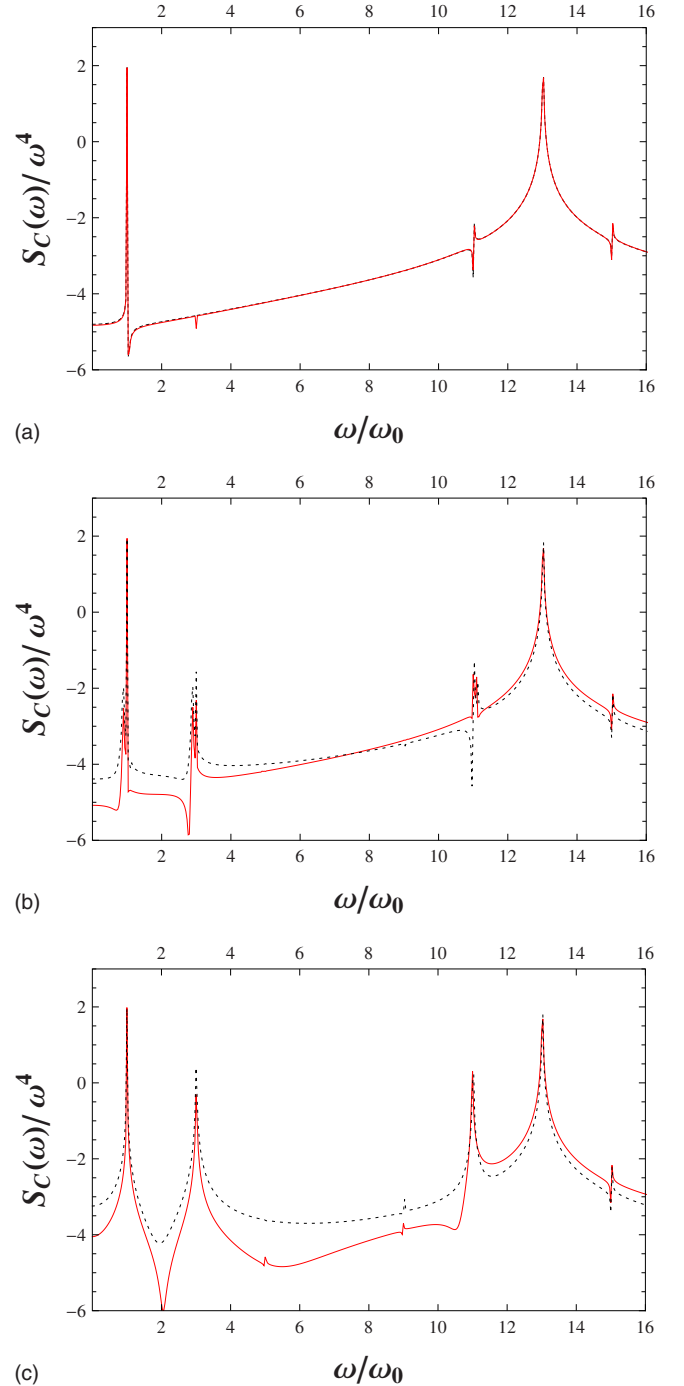
FIG. 2. (Color online) Scaled coherent spectra, $S_c(\omega)/\omega^4$, produced by 30-cycle pulse of square envelope: (a) two-level system with $\omega_{21}/\omega_0 = 13$ and $\Omega_R/\omega_0 = 0.5$, (b) three-level lambda system with the same ω_{21} and Ω_R values as for the two-level system and, additionally, $\omega_{23}/\omega_0 = 11.12$, $\omega_{31}/\omega_0 = 1.88 \rightarrow \delta_0 = \omega_{31} - 2\omega_0 = -0.12\omega_0$, and $M_R/\omega_0 = 0.3$, and (c) as (b) but with $\omega_{23}/\omega_0 = 11$ and $\omega_{31}/\omega_0 = 2 \rightarrow \delta_0 = 0$. Solid (dotted) curve—analytical (numerical) spectrum.

$|\rho(t)|^2 \leq 0.4$] and thus one observes some discrepancies between the curves concerning the height of the background mainly. The reason of these discrepancies is the effect of multiphoton coherent population trapping in the superposition of states $|1\rangle$ and $|3\rangle$ (~ 0.71 population in

$|1\rangle$, ~ 0.29 population in $|3\rangle$, and, practically, no population in $|2\rangle$). We will give more attention to this effect elsewhere.

The changes in the scaled spectrum around ω_0, $3\omega_0$, and $\omega_{21} - 2\omega_0$, caused by the third level under the condition of two-photon $1 \rightarrow 3$ resonance, $\omega_{31} \approx 2\omega_0$, are a special case of more general multiphoton (even-photon) resonance when the ω_{31} distance is close to the total energy of an even number of photons. Still keeping ω_{31} positive, one finds that the dominant terms in $d_\rho(t)$ are then those accompanied by $f_{-2-m} J_0(x_1) J_{-m}(x_1)$ with m non-negative. If $\omega_{31} \approx 2(m+1)\omega_0$, these terms lead to

$$
\begin{aligned}
d_\rho(t) = \frac{\mu_{23}}{4} \frac{M_R \Omega_R^2}{\omega_{21}^2} (-1)^m \frac{(x_1/2)^m}{m!} \frac{1}{\delta_m + \dfrac{\Delta_s}{2}} \Bigg\{ \cos(\omega_{31} - \omega_0 \\
- \delta_m)t - \cos\left(\omega_{31} - \omega_0 + \frac{\Delta_s}{2}\right)t + \cos(\omega_{31} + \omega_0 - \delta_m)t \\
- \cos\left(\omega_{31} + \omega_0 + \frac{\Delta_s}{2}\right)t + 2\cos\left(\omega_{23} - \frac{\Delta_s}{2}\right)t \\
- 2\cos(\omega_{23} + \delta_m)t \Bigg\},
\end{aligned}
\tag{43}
$$

where $\delta_m = \omega_{31} - 2(m+1)\omega_0$ is the static detuning from $2(m+1)$-photon $1 \rightarrow 3$ resonance. As seen, Eq. (42) is a special form of Eq. (43) when $m = 0$. For $\delta_m \rightarrow -\Delta_s/2$, the coefficients at the cosine functions in Eq. (43) become higher than the appropriate coefficients in Eq. (26) for $d_1(t)$. For a given $m > 0$, Eq. (43) thus predicts the appearance of resonance structures in the scaled spectrum around $\omega_{31} \pm \omega_0$ and ω_{23}. These predicted resonance structures are marked by arrows in Fig. 3 showing scaled spectra for two different $\omega_{31} > 0$ separations ($4\omega_0$ and $6\omega_0$, meaning $m = 1$ and $m = 2$, respectively). As previously, the solid (dotted) curves are the analytic (numerical) scaled spectra. Let us notice that, for $m > 0$, the satellites $\omega_{21} \pm 2\omega_0$ of the transition frequency ω_{21} keep the same height just opposite to the case of $m = 0$, i.e., $\omega_{31} \approx 2\omega_0$.

We would like to stress that some peaks in Fig. 3 have interference character. A good example of this interference is the third harmonic peak ($3\omega_0$) formed in the case of the level separation frequency $\omega_{31} = 4\omega_0$. In fact, this peak has two origins: the off-resonance and resonance ones. The off-resonance contribution comes from Eq. (41) for $d_1(t)$. The resonance contribution is given by Eq. (43) when taking $m = 1$. This resonance contribution is simply the left (low-frequency) wing of the doublet $\omega_{31} \pm \omega_0$ built up around the separation frequency ω_{31}. In Fig. 4, we show the interference structure of the third harmonic peak by changing the separation frequency ω_{31} slightly around $4\omega_0$. The single peak at $3\omega_0$, well pronounced in Fig. 3(a) when $\omega_{31} = 4\omega_0$, is seen in Fig. 4 to split into two components when one departs from the perfect four-photon ω_{31} separation. The weaker component (the off-resonance one) keeps the position $3\omega_0$, irrespective of the choice of ω_{31}, while the stronger component (the resonance one) moves to the position $\omega_{31} - \omega_0$.
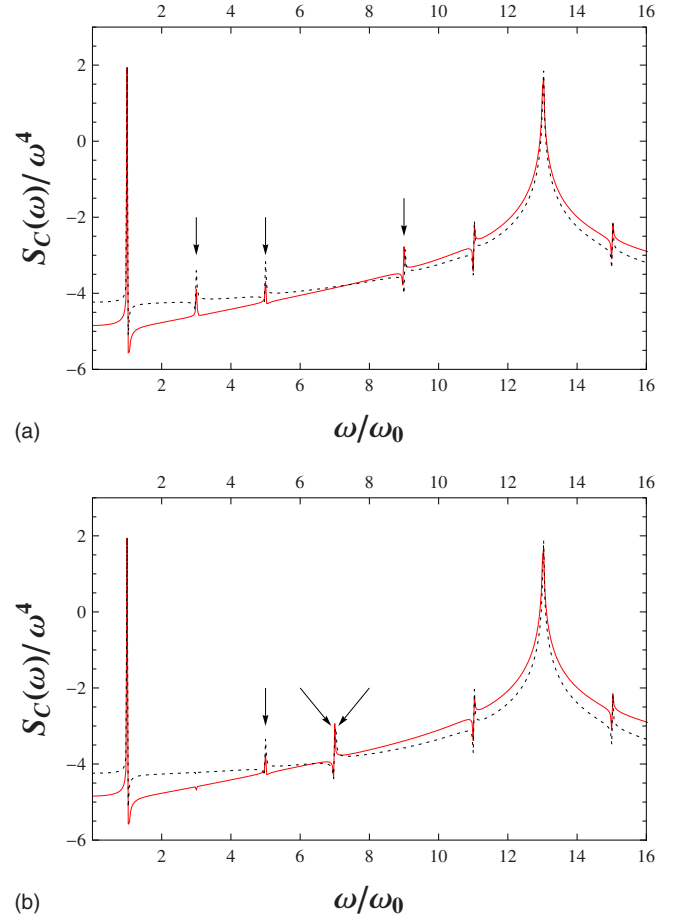
FIG. 3. (Color online) Scaled coherent spectra from three-level lambda systems of different even-photon level separations $\omega_{31} > 0$: (a) $\omega_{31}/\omega_0 = 4$; (b) $\omega_{31}/\omega_0 = 6$. Other parameters: $\omega_{21}/\omega_0 = 13$, $\Omega_R/\omega_0 = 0.5$, and $M_R/\omega_0 = 0.3$. The arrows indicate the resonantly enhanced spectral components $\omega_{31} \pm \omega_0$ and ω_{23}. In (b), the component $\omega_{31} + \omega_0$ overlaps with the component ω_{23}.

Let us consider now the case when, instead of even-photon $1 \rightarrow 3$ resonance, one realizes the vicinity of odd-photon $3 \rightarrow 2$ resonance, still being far from odd-photon $1 \rightarrow 2$ resonance. Assuming ω_{23} to be positive (lambda system) and close to $(2p+1)$-photon resonance, with p being non-negative, one finds g_p of Eq. (40) as the largest coefficient. Then the leading terms in $d_\rho(t)$ are those proportional to $g_p J_0(x_1) J_p(x_1)$, giving

$$
\begin{aligned}
d_\rho(t) = \frac{\mu_{23}}{4} \frac{M_R \Omega_R^2}{\omega_{21}^2} \frac{(x_1/2)^p}{p!} \frac{2}{\Delta_p - \dfrac{\Delta_s}{2}} \Bigg\{ \cos(\omega_{31} - \omega_0 + \Delta_p)t \\
- \cos\left(\omega_{31} - \omega_0 + \frac{\Delta_s}{2}\right)t + \cos(\omega_{31} + \omega_0 + \Delta_p)t \\
- \cos\left(\omega_{31} + \omega_0 + \frac{\Delta_s}{2}\right)t + 2\cos\left(\omega_{23} - \frac{\Delta_s}{2}\right)t \\
- 2\cos(\omega_{23} - \Delta_p)t \Bigg\},
\end{aligned}
\tag{44}
$$
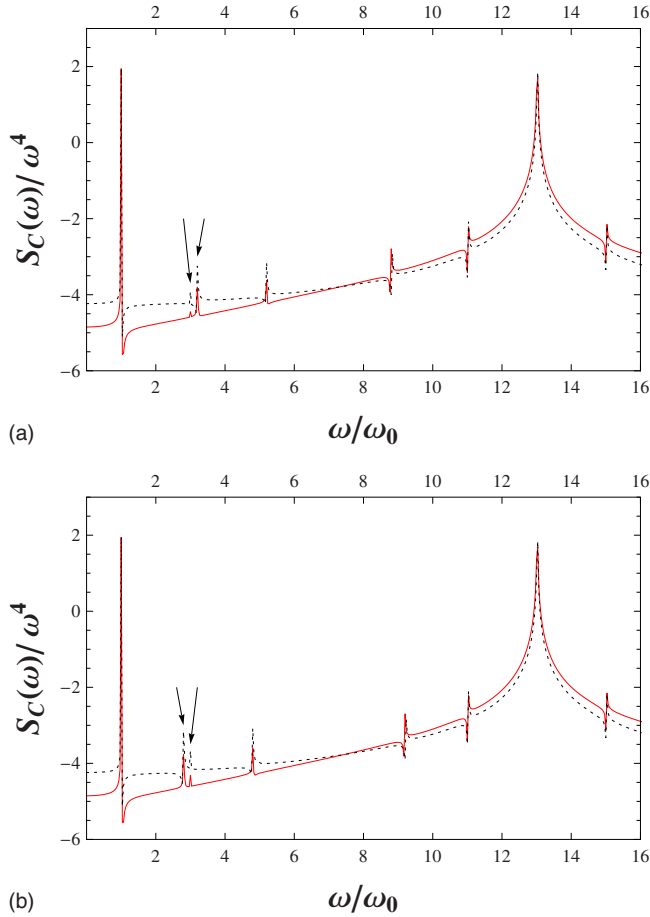
FIG. 4. (Color online) Splitting of the third-harmonic peak from Fig. 3(a) into two components when changing the level separation ω_{31} around $4\omega_0$: (a) $\omega_{31}/\omega_0=4.2$; (b) $\omega_{31}/\omega_0=3.8$. Other parameters: $\omega_{21}/\omega_0=13$, $\Omega_R/\omega_0=0.5$, and $M_R/\omega_0=0.3$. The arrows indicate the interfering spectral components.

where $\Delta_p=\omega_{23}-(2p+1)\omega_0$ stands for the static detuning from $(2p+1)$-photon $3\rightarrow2$ resonance. Since Eq. (44) is of the same structure as Eq. (43), it will generate spectra similar to those discussed earlier but with different positions of the $\omega_{31}\pm\omega_0$ and ω_{23} peaks.

The special case of interest is that of two coupled multiphoton resonances, i.e., when both the even-photon $1\rightarrow3$ and odd-photon $3\rightarrow2$ resonances take place simultaneously $(\delta_m\rightarrow-\Delta_s/2,\Delta_p\rightarrow\Delta_s/2)$. Then, the resonant part of the scaled spectrum is determined by the sum of Eqs. (43) and (44). Due to the weak-field condition, $x_1\ll1$, these two equations will, however, contribute comparably if $m=p$ only, otherwise either Eq. (43) or (44) dominates. This comparable-contribution condition requires $(2p+2)$-photon $1\rightarrow3$ resonance and $(2p+1)$-photon $3\rightarrow2$ resonance simultaneously. In this case, the $\omega_{31}-\omega_0$ spectral component will always interfere with the ω_{23} component. As compared to the single-resonance case, the spectrum is thus expected to be reduced by one peak, generally, when approaching two coupled resonances. Now, the well pronounced lines, caused by the third level, should be $\omega_{31}+\omega_0=(2p+3)\omega_0$ and $\omega_{31}-\omega_0=\omega_{23}=(2p+1)\omega_0$. The effect of two coupled resonances is shown in Fig. 5(a) for $m=p=3$, i.e., eight-photon $1\rightarrow3$
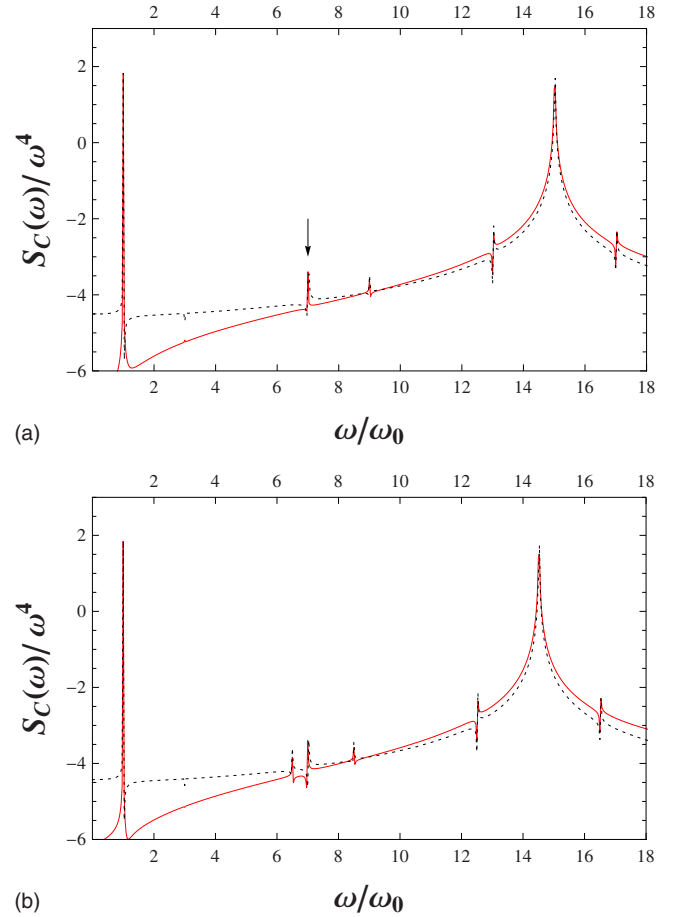
FIG. 5. (Color online) Reduction in the number of spectral lines in the scaled coherent spectrum from three-level lambda system when approaching two coupled resonances, i.e., even-photon $1\rightarrow3$ and odd-photon $3\rightarrow2$ resonances simultaneously: (a) the case of eight-photon $1\rightarrow3$ resonance ($\omega_{31}/\omega_0=8$) plus seven-photon $3\rightarrow2$ resonance ($\omega_{23}/\omega_0=7$). Other parameters: $\omega_{21}/\omega_0=15$, $\Omega_R/\omega_0=0.5$, and $M_R/\omega_0=0.3$. (b) The case of some detuning from eight-photon $1\rightarrow3$ resonance ($\omega_{31}/\omega_0=7.5$) plus seven-photon $3\rightarrow2$ resonance ($\omega_{23}/\omega_0=7$). Other parameters: $\omega_{21}/\omega_0=14.5$, $\Omega_R/\omega_0=0.5$, and $M_R/\omega_0=0.3$. The arrow shows where the $\omega_{31}-\omega_0$ and ω_{23} components overlap.

resonance ($\delta_3=0$) and seven-photon $3\rightarrow2$ resonance ($\Delta_3=0$) simultaneously. The reduction in the number of lines in the scaled spectrum, due to coupled resonances, is seen by comparing Fig. 5(a) with Fig. 5(b), the latter one prepared for substantial detuning $\delta_3=\omega_{31}-8\omega_0=-0.5\omega_0$ from eight-photon $1\rightarrow3$ resonance. Obviously, the case of two coupled resonances means also the odd-photon $1\rightarrow2$ resonance of high order $k=2(m+1)+(2p+1)=2(m+p)+3$. The term describing this resonance is that proportional to $b_rJ_r(x_2)J_0(x_2)$ in Eq. (26) for $d_1(t)$, where $r=(k-1)/2=m+p+1$. This term can result in eventual enhancements of the ω_{21} and $2\omega_{21}-(2r+1)\omega_0$ components eventually.

The scaled coherent spectra of Figs. 2–5 were obtained under the assumption of square pulse. In Sec. III A, we have, however, predicted substantial suppression of some spectral components when applying smooth pulse instead of a square pulse. Figure 6, when compared with Fig. 2(b), shows an
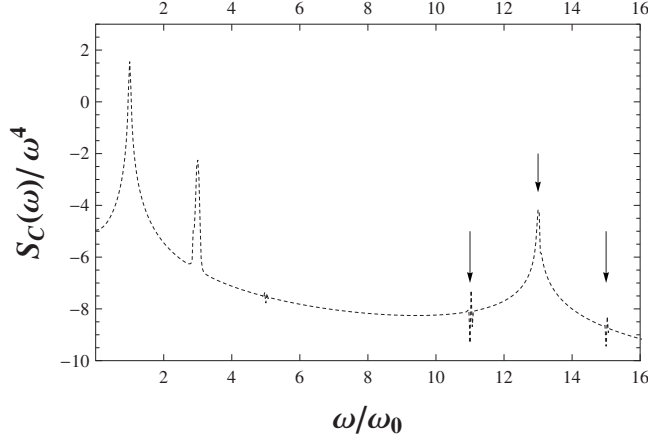
FIG. 6. Suppression of selected spectral components in the scaled coherent spectrum (those indicated by the arrows) when replacing square pulse, $f(t)=1$, by a smooth pulse, $f(t)=\sin(\Delta_l t)$, where $\Delta_l = \pi/t_p = \pi/(30T) = \omega_0/60$. Other parameters as in Fig. 2(b). The present spectrum was obtained by solving numerically Eqs. (3) and putting the solution into Eq. (5).

exemplifying pulse-shape effect in the scaled coherent spectrum. The numerical spectrum of Fig. 6 was obtained for the same parameters as Fig. 2(b) except the pulse shape being now $f(t)=\sin(\Delta_l t)$, where $\Delta_l = \pi/t_p = \pi/30T = \omega_0/60$. The arrows in Fig. 6 indicate the suppressed spectral components. Figure 6 confirms the analytic predictions of Sec. III A concerning both the suppressed components [those governed by the term proportional to $e^{-i\omega_{21}t}$ in r_0 of Eq. (23)] and the degree of suppression (of the order $(\Delta_l/\omega_{21})^2 = [(\omega_0/\omega_{21})(\Delta_l/\omega_0)]^2 = [(1/13)(1/60)]^2 = 1.6 \times 10^{-6}$). The square-pulse approximation is thus seen to overestimate greatly some frequency components in the coherent spectra. Moreover, the components ω_0 and $3\omega_0$ are spectrally wider in Fig. 6 than in Fig. 2(b) and do not exhibit the doublet structures as it was for square pulse.

IV. TOTAL SPECTRUM

To calculate the total spectrum we first need to find its incoherent part [$j=2$ and 3 in Eqs. (1), (2), and (3a)–(3c)] and then add this part to the coherent part calculated in Sec. III. In contrast to the coherent part, determined completely by the ratios r and ρ only, one now needs to know all population amplitudes b_{kj} found at the initial conditions indicated by $j=1$, 2, and 3.

For $j=1$, Eqs. (3) can be solved in terms of r and ρ as

$$b_{11}(t) = e^{-i[\omega_1 t - A(t)]}, \tag{45}$$

$$b_{21}(t) = ie^{-i\omega_2 t} \int_0^t [\Omega(t') + M(t')\rho(t')]b_{11}(t')e^{i\omega_2 t'} dt', \tag{46}$$

$$b_{31}(t) = ie^{-i\omega_3 t} \int_0^t M(t')b_{21}(t')e^{i\omega_3 t'} dt', \tag{47}$$

where $A(t) = \int_0^t r(t')\Omega(t')dt'$ is a generalization of Eq. (16) for $A_0(t)$. In a general case, r and ρ have to be found from exact equations [Eqs. (7)].

For $j=3$, we introduce different ratios, $x=b_{23}/b_{33}$ and $y=b_{13}/b_{33}$. From Eqs. (3), we find equations for them symmetric to Eqs. (7) for r and ρ, namely,

$$i\frac{dx}{dt} = (x^2 - 1)M(t) + \omega_{23}x - \Omega(t)y, \tag{48a}$$

$$i\frac{dy}{dt} = [\omega_{13} + M(t)x]y - \Omega(t)x. \tag{48b}$$

In terms of x and y, the set of Eqs. (3) has the solutions

$$b_{33}(t) = e^{-i[\omega_3 t - B(t)]}, \tag{49}$$

$$b_{23}(t) = ie^{-i\omega_2 t} \int_0^t [M(t') + \Omega(t')y(t')]b_{33}(t')e^{i\omega_2 t'} dt', \tag{50}$$

$$b_{13}(t) = ie^{-i\omega_1 t} \int_0^t \Omega(t')b_{23}(t')e^{i\omega_1 t'} dt', \tag{51}$$

where $B(t) = \int_0^t x(t')M(t')dt'$.

Finally, for $j=2$, we define the ratios $u=b_{12}/b_{22}$ and $v=b_{32}/b_{22}$. These ratios are found from Eqs. (3) to satisfy the set of differential equations,

$$i\frac{du}{dt} = (u^2 - 1)\Omega(t) + [\omega_{12} + M(t)v]u, \tag{52a}$$

$$i\frac{dv}{dt} = (\vartheta^2 - 1)M(t) + [\omega_{32} + \Omega(t)u]v. \tag{52b}$$

Both equations in this set resemble, to some extent, Eq. (7a) for r and Eq. (48a) for x. In the case of $j=2$, the solutions of Eqs. (3), expressed through u and v, look like

$$b_{22}(t) = e^{-i[\omega_2 t - C(t) - D(t)]}, \tag{53}$$

$$b_{12}(t) = ie^{-i\omega_1 t} \int_0^t \Omega(t')b_{22}(t')e^{i\omega_1 t'} dt', \tag{54}$$

$$b_{32}(t) = ie^{-i\omega_3 t} \int_0^t M(t')b_{22}(t')e^{i\omega_3 t'} dt', \tag{55}$$

where $C(t) = \int_0^t u(t')\Omega(t')dt'$ and $D(t) = \int_0^t v(t')M(t')dt'$.

Now, we adapt the above formal solutions to the weak-field low-frequency excitation by square pulse, i.e., the conditions under which we have calculated analytically the coherent part of the spectrum in Sec. III. The condition of weak field, translating into weak depopulation of the initial state, allows us to neglect the term $M(t')\rho(t')$ in Eq. (46) for b_{21} and to replace $r(t')$ by $r_0(t')$ implying the replacement $A(t) \rightarrow A_0(t)$, where $A_0(t)$ is given by Eq. (20). Similarly, we can drop out the term $\Omega(t')y(t')$ in Eq. (50) for b_{23} and replace $B(t)$ by $B_0(t) = \int_0^t x_0(t')M(t')dt'$, where the equation for x_0 is obtained from Eq. (48a) in the same way as Eq. (10) for r_0 from Eq. (7a). In the low-frequency limit ($\omega_0 \ll |\omega_{23}|$ in this case), $B_0(t)$ is thus found from Eq. (20) for $A_0(t)$ by replacing
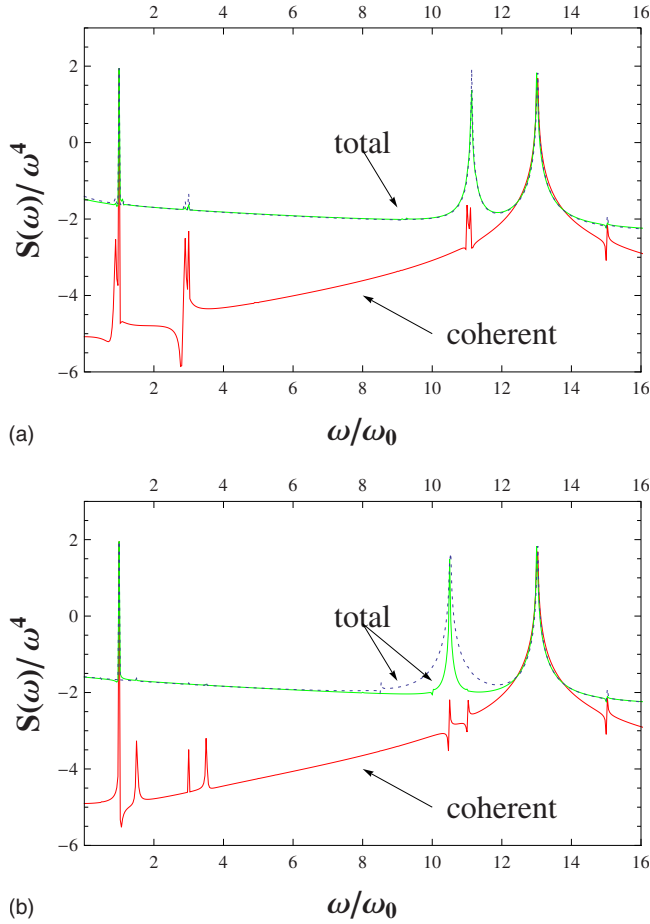
FIG. 7. (Color online) Scaled total spectrum calculated from the analytical amplitudes [Eqs. (56)–(64)] (solid curve) in comparison with the numerical total spectrum (dotted curve). The bottom curve is the coherent spectrum. (a) The same parameters as in Fig. 2(b); (b) the parameters as in (a) except $\omega_{23}/\omega_0 = 10.5$.

$\Omega_R \rightarrow M_R$ and $\omega_{21} \rightarrow \omega_{23}$ simultaneously. Finally, we are allowed to ignore the terms $M(t)v$ in Eq. (52a) and $\Omega(t)u$ in Eq. (52b) obtaining a pair of decoupled Riccati-type equations in which we then neglect the inherent quadratic terms. From Eqs. (52), approximated along the above lines, we find $u_0(t)$ and $v_0(t)$ and use these solutions to replace $C(t) \rightarrow C_0(t) = \int_0^t u_0(t')\Omega(t')dt' = -A_0(t)$ and $D(t) \rightarrow D_0(t) = \int_0^t v_0(t')M(t')dt' = -B_0(t)$. All these approximations, along with the Fourier-Bessel expansion such as Eq. (21), result in the analytic amplitudes given in the Appendix.

From Eqs. (1) and (2) and the analytic amplitudes, we finally find the total spectrum of scattered light, i.e., that composed of both the coherent and incoherent parts. In Fig. 7, we present the exemplifying scaled total spectra, $S(\omega)/\omega^4$, obtained in this way (solid curves) and compare them with the numerical spectra (dotted curves), i.e., those based on numerical solution of Eqs. (3) for the amplitudes. The analytic total spectra are seen to reproduce well the numerical ones.

In both Figs. 7(a) and 7(b), we have included the corresponding coherent spectra as well. By comparing the total and coherent spectra, we see a profound effect of incoherency. Many details of the coherent spectrum are seen to dis-

appear almost completely in the total spectrum. This is due to the featureless, to some extent, intense background introduced by the incoherent part to the total spectrum. For the parameters taken, the total spectrum includes practically three components only, ω_0, ω_{21}, and ω_{23}, with the latter one being enhanced as compared with that in the coherent spectrum.

To observe the predicted details of the coherent spectra in a real experiment, dealing with a large collection of identical three-level systems rather than one, it is thus recommended to choose the forward direction of observation. The reason is that the coherent part of the forward-scattered light from a macroscopic sample is proportional to the second power of the number of individual systems but the incoherent part is proportional only linearly to this number [20].

V. SUMMARY

In the approximate analytical approach, we have calculated the spectrum of light scattered by a three-level system. The pulsed classical light, of duration much shorter than the spontaneous-decay time, was assumed to be weak ($\Omega_R/\omega_{21} \ll 1$) and of low frequency ($\omega_0/\omega_{21} \ll 1$). Physically, the weak field was understood as that depopulating weakly the initial state, and the low frequencies were those allowing high-order multiphoton transitions in the system. Our approach was based on a pair of coupled differential equations for the appropriately defined ratios of the level-population amplitudes with one equation, at least, being the Riccati-type one. We have calculated the total spectrum, i.e., both its coherent and incoherent parts. We have put special emphasis on description of the coherent part of the spectrum from the lambda-type system under the conditions of multiphoton resonances between different levels, including the case of two coupled resonances as well. Moreover, profound effect of the incoherent part on the total spectrum was found. Generally, many details of the coherent spectrum were shown to vanish in the total spectrum due to substantial featureless background coming from the incoherent part. By comparison with numerical spectra our analytic approach was proved to be good. We have recommended the forward direction of observation in a real scattering experiment to verify the predictions of our theory.

APPENDIX

The amplitudes calculated along the line sketched in Sec. IV are

$$b_{11}(t) = e^{-i(\omega_1 - \Delta_s/2)t} \sum_{m=-\infty}^{+\infty} J_m(x_1)e^{i2m\omega_0 t}, \qquad (A1)$$

$$b_{21}(t) = \frac{1}{2}\Omega_R e^{-i\omega_2 t} \sum_{m=-\infty}^{+\infty} \alpha_m[J_m(x_1) + J_{m+1}(x_1)]$$

$$\times \{e^{i[\omega_{21} + (2m+1)\omega_0 + \Delta_s/2]t} - 1\}, \qquad (A2)$$

$$b_{31}(t) = \frac{1}{4} M_R \Omega_R e^{-i\omega_3 t} \sum_{m=-\infty}^{+\infty} \{[\alpha_m \beta_m J_m(x_1) + \alpha_{m+1} \beta_m J_{m+2}(x_1)$$

$$+ (\alpha_m + \alpha_{m+1}) \beta_m J_{m+1}(x_1)] \{e^{i[\omega_{31} + 2(m+1)\omega_0 + \Delta_s/2]t} - 1\}$$

$$+ (\alpha_m + \alpha_{m-1}) J_m(x_1) \{\gamma_- [e^{-i(\omega_{23} - \omega_0)t} - 1]$$

$$+ \gamma_+ [e^{-i(\omega_{23} + \omega_0)t} - 1]\}\}, \tag{A3}$$

$$b_{33}(t) = e^{-i(\omega_3 - \Delta_s'/2)t} \sum_{m=-\infty}^{+\infty} J_m(x_1') e^{i2m\omega_0 t}, \tag{A4}$$

$$b_{23}(t) = \frac{1}{2} M_R e^{-i\omega_2 t} \sum_{m=-\infty}^{+\infty} \bar{\alpha}_m [J_m(x_1') + J_{m+1}(x_1')]$$

$$\times \{e^{i[\omega_{23} + (2m+1)\omega_0 + (\Delta_s'/2)]t} - 1\}, \tag{A5}$$

$$b_{13}(t) = \frac{1}{4} M_R \Omega_R e^{-i\omega_1 t} \sum_{m=-\infty}^{+\infty} \{[\bar{\alpha}_m \bar{\beta}_m J_m(x_1') + \bar{\alpha}_{m+1} \bar{\beta}_m J_{m+2}(x_1')$$

$$+ (\bar{\alpha}_m + \bar{\alpha}_{m+1}) \bar{\beta}_m J_{m+1}(x_1')] \{e^{i[\omega_{13} + 2(m+1)\omega_0 + \Delta_s'/2]t} - 1\}$$

$$+ (\bar{\alpha}_m + \bar{\alpha}_{m-1}) J_m(x_1') \{\bar{\gamma}_- [e^{-i(\omega_{21} - \omega_0)t} - 1]$$

$$+ \bar{\gamma}_+ [e^{-i(\omega_{21} + \omega_0)t} - 1]\}\}, \tag{A6}$$

$$b_{22}(t) = e^{-i(\omega_2 + \Delta_s/2 + \Delta_s'/2)t} \sum_{m=-\infty}^{+\infty} J_m(x_1 + x_1') e^{-i2m\omega_0 t}, \tag{A7}$$

$$b_{12}(t) = -\frac{1}{2} \Omega_R e^{-i\omega_1 t} \sum_{m=-\infty}^{+\infty} \alpha_m' [J_m(x_1 + x_1') + J_{m+1}(x_1 + x_1')]$$

$$\times \{e^{i[\omega_{21} + (2m+1)\omega_0 + \Delta_s/2 + \Delta_s'/2]t} - 1\}, \tag{A8}$$

$$b_{32}(t) = -\frac{1}{2} M_R e^{-i\omega_3 t} \sum_{m=-\infty}^{+\infty} \bar{\alpha}_m' [J_m(x_1 + x_1') + J_{m+1}(x_1 + x_1')]$$

$$\times \{e^{-i[\omega_{23} + (2m+1)\omega_0 + \Delta_s/2 + \Delta_s'/2]t} - 1\}, \tag{A9}$$

where

$$\alpha_m = \frac{1}{\omega_{21} + (2m+1)\omega_0 + \dfrac{\Delta_s}{2}}, \tag{A10}$$

$$\beta_m = \frac{1}{\omega_{31} + 2(m+1)\omega_0 + \dfrac{\Delta_s}{2}} = f_m, \tag{A11}$$

$$\gamma_\pm = \frac{1}{\omega_{23} \pm \omega_0}, \tag{A12}$$

$$\bar{\alpha}_m = \frac{1}{\omega_{23} + (2m+1)\omega_0 + \dfrac{\Delta_s'}{2}}, \tag{A13}$$

$$\bar{\beta}_m = \frac{1}{\omega_{13} + 2(m+1)\omega_0 + \dfrac{\Delta_s'}{2}}, \tag{A14}$$

$$\bar{\gamma}_\pm = \frac{1}{\omega_{21} \pm \omega_0}, \tag{A15}$$

$$\alpha_m' = \frac{1}{\omega_{21} + (2m+1)\omega_0 + \dfrac{\Delta_s}{2} + \dfrac{\Delta_s'}{2}}, \tag{A16}$$

$$\bar{\alpha}_m' = \frac{1}{\omega_{23} + (2m+1)\omega_0 + \dfrac{\Delta_s}{2} + \dfrac{\Delta_s'}{2}} \tag{A17}$$

and, moreover, $x_1 = \Omega_R^2/(4\omega_0\omega_{21})$, $x_1' = M_R^2/(4\omega_0\omega_{23})$, $\Delta_s = \Omega_R^2/\omega_{21}$, and $\Delta_s' = M_R^2/\omega_{23}$. For low frequencies of interest ($\omega_0 \ll \omega_{21}, |\omega_{23}|$) the denominators in these coefficients can be approximated properly. Then, some of the above coefficients become identical.

[1] G. N. Gibson, Phys. Rev. Lett. **89**, 263001 (2002); Phys. Rev. A **67**, 043401 (2003).

[2] H. K. Avetissian and G. F. Mkrtchian, Phys. Rev. A **66**, 033403 (2002).

[3] H. K. Avetissian, B. R. Avchyan, and G. F. Mkrtchian, Phys. Rev. A **74**, 063413 (2006); **77**, 023409 (2008).

[4] H. K. Avetissian, G. F. Mkrtchian, and M. G. Poghosyan, Phys. Rev. A **73**, 063413 (2006).

[5] A. R. P. Rau and W. Zhao, Phys. Rev. A **68**, 052102 (2003); **71**, 063822 (2005).

[6] B. Sundaram and P. W. Milonni, Phys. Rev. A **41**, 6571 (1990).

[7] L. Plaja and L. Roso-Franco, J. Opt. Soc. Am. B **9**, 2210 (1992).

[8] K. J. LaGattuta, J. Mod. Opt. **39**, 1181 (1992).

[9] T. Zuo, S. Chelkowski, and A. D. Bandrauk, Phys. Rev. A **49**, 3943 (1994).

[10] M. Yu. Ivanov and P. B. Corkum, Phys. Rev. A **48**, 580 (1993).

[11] M. Yu. Ivanov, P. B. Corkum, and P. Dietrich, Laser Phys. **3**, 375 (1993).

[12] R. Bavli and H. Metiu, Phys. Rev. Lett. **69**, 1986 (1992); R. Bavli and Y. Dakhnovskii, Phys. Rev. A **48**, R886 (1993).

[13] A. Levinson, M. Segev, G. Almogy, and A. Yariv, Phys. Rev. A **49**, R661 (1994).

[14] S. Hughes, Phys. Rev. A **62**, 055401 (2000).

[15] T. Tritschler, O. D. Mücke, and M. Wegener, Phys. Rev. A **68**, 033404 (2003).

[16] T. Tritschler, O. D. Mücke, M. Wegener, U. Morgner, and F. X. Kärtner, Phys. Rev. Lett. **90**, 217404 (2003).

[17] R. Parzyński and M. Sobczak, J. Phys. B **37**, 743 (2004).

[18] A. Plucińska and R. Parzyński, J. Mod. Opt. **54**, 745 (2007).

[19] P. Caldara and E. Fiordilino, J. Mod. Opt. **46**, 743 (1999).

[20] J. H. Eberly and M. V. Fedorov, Phys. Rev. A **45**, 4706 (1992).

[21] D. G. Lappas, M. V. Fedorov, and J. H. Eberly, Phys. Rev. A **47**, 1327 (1993).

[22] D. L. Powers, *Elementary Differential Equations with Boundary Value Problems* (P.W.S., Boston, 1985).

[23] I. S. Gradshteyn and I. M. Ryzhik, *Tables of Integrals Series and Products* (Academic Press, New York, 2000).